Chalcogenide Letters Vol. 15, No. 5, May 2018, p. 267 - 279

EFFECT OF 80 MeV Si SWIFT HEAVY ION IRRADIATION ON $Ge_{22}Se_{78}$ THIN FILMS FOR OPTICAL APPLICATIONS

R. CHAUHAN[a], S. PANDEY[a], S. G. PRASAD[b]
[a]*Department of Physics, D.A-V. College, CSJM University, Kanpur 208001, India*
[b]*Department of Chemistry, Uttar Pradesh Textile Technology Institute, Kanpur 208001, India*

Present study reports about changes in optical properties of amorphous intermediate phase $Ge_{22}Se_{78}$ thin films under 80 MeV Si swift heavy ion (SHI) for six different fluences ($3x10^{10}$, $1x10^{11}$, $3x10^{11}$, $1x10^{12}$, $3x10^{12}$, $1x10^{13}$ ions/cm^2). Linear optical properties are determined from optical transmission spectrum using Swanepoel method. The dispersion in the thin film is determined by the Wemple-DiDomenico relation. Tauc's parameter and optical band gap are determined by extrapolating Tauc's plot for indirect band gap material. The nonlinear susceptibility is determined by the Miller's Rule. The nonlinear refractive index is determined by the Ticha and Tichy relation. The changes in thin films morphology are explained by SEM images and it is observed that the fluence $1x10^{13}$ ions/cm^2 is the upper limit of ion treatment. The linear refractive index increases from 1.97 to 2.16 up to fluence $3x10^{12}$ ions/cm^2, and then reduces to 2.11 up to fluence $1x10^{13}$ ions/cm^2. The optical band gap decreases from 1.99 eV to 1.94 eV up to fluence $3x10^{12}$ ions/cm^2, and then increases to 2.01 eV up to fluence $1x10^{13}$ ions/cm^2. The nonlinear refractive index increases from $8.038x10^{-11}$ [esu] to $8.895x10^{-11}$ [esu] up to fluence $3x10^{12}$ ions/cm^2, and then reduces to $7.696x10^{-11}$ [esu] up to fluence $1x10^{13}$ ions/cm^2. Changes in optical properties due ion irradiation are explained by structural changes with the help of Raman measurements. It shows that SHI is an effective technique to change the properties of amorphous chalcogenide thin films according to the need of the optical/photonic applications.

(Received February 25, 2018; Accepted May 14, 2018)

Keywords: Amorphous chalcogenides; Thin films; Swift heavy ion (SHI); Ion irradiation; Linear and nonlinear optical properties; Swanepoel method; Raman measurements

1. Introduction

Amorphous chalcogenide thin films are emerged as the potential candidate for photovoltaic applications [1, 2], nonlinear optical waveguide [3], radiation shielding [4], resistive RAM devices [5] and various IR optical/photonic applications [6]. Optical properties such as linear/nonlinear refractive index, optical band gap and optical loss play a key role while designing applications [7]. The glassy systems are categorized in three phases. These phases are a flexible-floppy phase, unstressed-rigid phase and stressed rigid phase [8], and are defined in terms of average coordinate number [9]. The average coordinate number of $Ge_{22}Se_{78}$ glass is 2.44 and belongs to unstressed-rigid phase (intermediate phase). Intermediate phase compositions are important from application point of view due to non-ageing behaviour [10].

Researchers use different techniques to modify the properties of amorphous chalcogenide thin films. Ion irradiation is a potential technique to tailor material properties. Energetic ions are divided into three categories, which are low energy ions, medium energy ions, and high energy ions. The energy of low energy ions lies in the range from few tens of KeV to hundreds of KeV. The energy of medium energy ions lies in the range from few hundreds of KeV to few tens of MeV. The energy of high energy ions lies in the range from few tens of MeV to a few GeV. High

*Corresponding author: chauhanrasmi@gmail.com

energy ions are also known as swift heavy ions (SHI) [11]. Low energy ions transfer energy to the material due to the elastic collision. This energy loss is known as nuclear energy loss of the order 10 KeV/amu. The nuclear energy loss is responsible for material modification. High energy ions transfer energy to the material by the inelastic collision. This energy loss is known as electronic energy loss of the order 1 Mev/amu. In the inelastic collision the energy transfer to the electron cloud and electron transfer energy to the lattice through electron-phonon interaction. The electronic energy loss is mainly responsible for the material properties modification. These changes depend upon the mass of incident ions, the mass of target material, and energy as well as fluence of the irradiated ions [12].

Kamboj *et al.* investigated GeSe thin films irradiated with the 60 MeV $^{12}C^{5+}$ ions of fluence 10^{12} and 10^{13} ions/cm^2. Due to effect of ion irradiation, optical band gap (E_g) decreased from 1.70 eV to 1.43 eV up to fluence 10^{13} ions/cm^2 [13]. Kumar *et al*. investigated 100 MeV Ag ion irradiation on $Ag_{0.10}(Ge_{0.20}Se_{0.80})_{0.90}$ thin films for fluence $1x10^{11}$ to $1x10^{13}$ ions/cm^2. The linear refractive index of this film increased at lower fluence $1x10^{11}$ ions/cm^2 and follows a reversal trend at higher fluences [14]. Dwivedi *et al.* reported comparative Raman study of GeSe thin films irradiated with 1 MeV Kr^{++} ions of fluence $2x10^{13}$ ions/cm^2 with white-light soaking. It was observed that structural changes by ion irradiation and light soaking did not follow similar trend. In case of ion irradiation, it indicated a reduction in disorder [10].

In the present study optical and structural properties of amorphous $Ge_{22}Se_{78}$ thin films are modified using ion irradiation technique for various optical/photonic applications. 80 MeV Si swift heavy ions (SHI) are used for six different fluences. These fluences are $3x10^{10}$ ions/cm^2 , $1x10^{11}$ ions/cm^2 , $3x10^{11}$ ions/cm^2 , $1x10^{12}$ ions/cm^2 , $3x10^{12}$ ions/cm^2 and $1x10^{13}$ ions/cm^2.

2. Experimental

The thin films of glassy alloy $Ge_{30}Se_{70}$ were prepared by vacuum evaporation technique. The thin films were deposited on the soda lime glass substrate. The soda lime glass substrate cleaned two times by Acetone and dried properly with wearing powder-free gloves. The film deposition carried out at room temperature inside coating system (HIND-HIVAC Model 12A 4DT) at the base pressure $3x10^{-5}$ mbar using molybdenum boat and current flow through the boat was 4.5 Ampere for 12 sec. The composition of the deposited thin film was $Ge_{22}Se_{78}$ by EDX analysis. The amorphous nature of the film was confirmed by the absence of any sharp peak using X-ray diffraction measurements (Bruker AXS T/T Horizontal Model 40KV/40 mA Cu Tube) with Cu Kα radiation at locked coupled scan type. The scan speed was 1^0/min and scan range 20^0 to 60^0 with increment 0.02. 80 MeV Si SHI irradiations were done using 15UD Pelletron tandem accelerator at Inter University Accelerator Center, New Delhi. The exposed area of the thin film was 1 cm^2 for six different fluences ($3x10^{10}$, $1x10^{11}$, $3x10^{11}$, $1x10^{12}$, $3x10^{12}$, $1x10^{13}$ ions/cm^2). Surface morphology of the films was determined using Scanning Electron Microscope (Oxford Instruments Inca Penta FETX3 Model 7718). The structural analysis of the thin films was done by micro-Raman measurements using spectrometer (Renishaw In Via Raman Microscope) with 515.4 nm Argon ion laser and power density 5mW/cm^2 at room temperature. The thickness of the film was measured by using thickness profilometer (KALOTENCORE Model D120). The optical transmission for normal incidence of the thin films was measured using a double beam UV/VIS computerised spectrophotometer (LABINDIA Model UV-3000) in the wavelength range 200-1100 nm with step size 1 nm.

3. Result and discussion

3.1 XRD measurements

XRD pattern of the pristine and irradiated thin film (at fluence $1x10^{13}$ ions/cm^2) is shown in Fig 1. Absence of any sharp peak in the XRD pattern of pristine and irradiated thin film indicates that amorphous nature of the thin films remains same after the SHI irradiation.

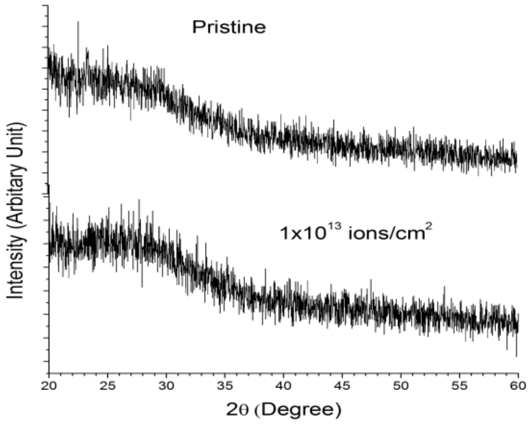

Fig. 1 XRD patterns of pristine and irradiated (1x10^{13} ions/cm^{2}) thin film

There is no hump appears in the pristine thin film, but a small hump is observed after irradiation. It indicates that small to medium range order generates in the thin films by the 80 MeV Si SHI irradiation [15].

3.2 SEM measurement

SEM images of the pristine and irradiated thin films (at fluence 1x10^{13} ions/cm^{2}) are shown in Fig 2. The investigation of the topography of the irradiated thin film indicates that bubbles are formed on the surface of the irradiated thin film. Due to the bubble formation, the surface of the irradiated thin film gets rougher. Some bubbles appear transparent and semi-transparent. The bubble formation or defect creation on the surface occurs due to electronic excitation. When the thin film is irradiated with ions, the electrons of the material get excited and become free for short duration. Due to electron-phonon interactions, the energy of electrons is distributed among other atoms of the material. After acquiring this energy, the cones of highly ionized plasma are generated on the thin film surface. These cones are very unstable due to the Coulomb's repulsion between electrostatic charges. After irradiation, these cones become distorted and transform into the size of bubbles [16]. These bubbles are used as the part of microelectronics and are known as microelectromechanical system (MEMS) [17]. Thus, 1x10^{13} ions/cm^{2} is the upper limit of SHI irradiation for this film. This is the indication of starting of destruction of the film. The properties should be modified below the upper limit of the fluence.

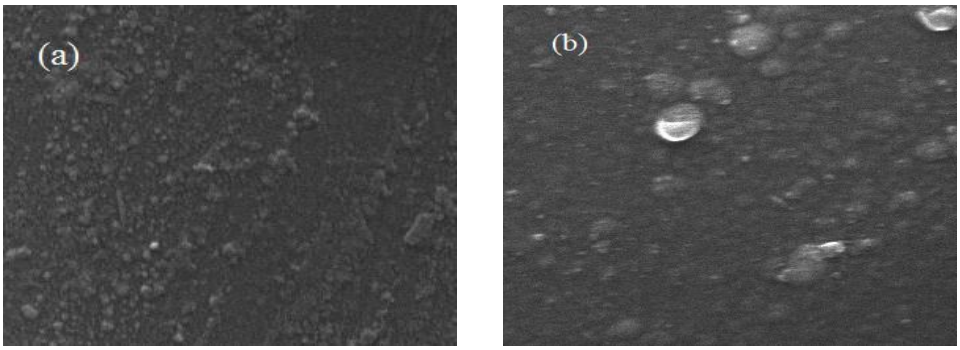

Fig. 2 SEM images (a) Pristine and (b) Irradiated thin film (1x10^{13} ions/cm^{2}) at 5 μm

3.3 Calculation of energy loss and stopping range

Energetic ions are used to change material structure by transferring the energy into the target material. Energy loss and stopping range of irradiated ions within the material are calculated using SRIM 2008 [18]. The calculation shows that 80 MeV Si ion have the nuclear energy loss

0.347 eV/Å and electronic energy loss 3.70×10^2 eV/Å in the amorphous $Ge_{22}Se_{78}$ thin film. From the above calculation, it is clear that nuclear energy loss is negligible compared to electronic energy loss. Hence, electronic energy loss gives major contribution in energy deposition inside the material due to SHI irradiation. The stopping range of the 80 MeV Si ions for the amorphous thin film sample is 20.29 μm. This stopping range is more than the film thickness (≈ 1.62 μm). Hence Si ions come into rest within the glass substrate after passing through the amorphous thin films.

3.4 Optical Analysis

In the present study, the changes in optical properties of thin film are determined by the numerical value of optical constant such as refractive index, absorption coefficient, extinction coefficient, and optical bandgap. The refractive index of thin film is calculated according to the method described by the Swanepoel [19, 20]. Origin 8.5 is used for finding peaks, and creating envelopes (upper and lower) on the optical transmission spectra. The upper and lower envelopes on the optical transmission spectra are shown in Fig 3.

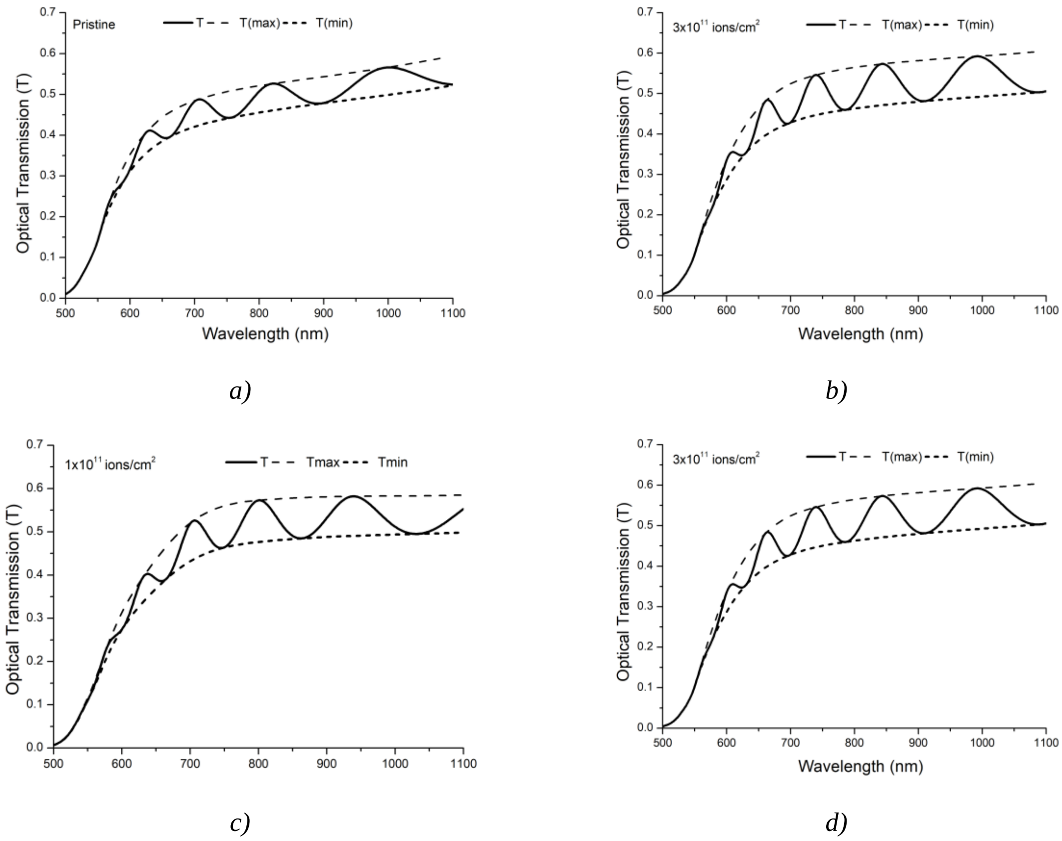

Fig. 3.1 Upper Envelope (T (Max)) and Lower Envelope (T (Min)) plots on the optical transmission spectra of the pristine and irradiated thin films:
(a) pristine; (b) $3x10^{10}$ ions/cm^2; (c) $1x10^{11}$ ions/cm^2; (d) $3x10^{11}$ ions/cm^2

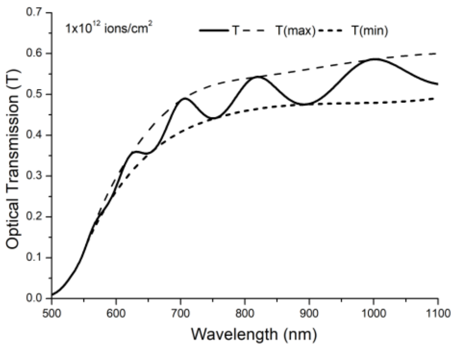

e)

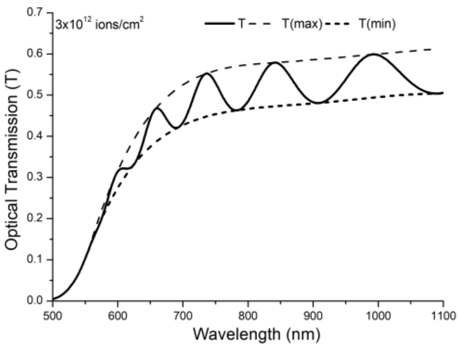

f)

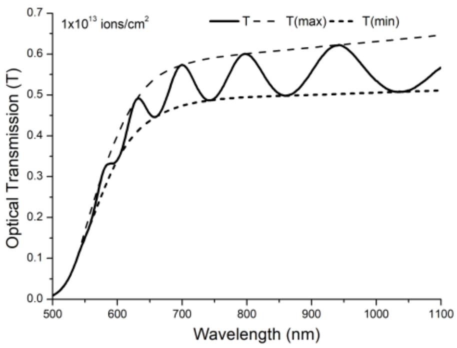

g)

Fig. 3.2 Upper Envelope (T (Max)) and Lower Envelope (T (Min)) plots on the optical transmission spectra of the pristine and irradiated thin films: (e) $1x10^{12}$ ions/cm^2; (f) $3x10^{12}$ ions/cm^2: (g) $1x10^{13}$ ions/cm^2

The calculated values of refractive index using Swanepoel method are fitted by the Cauchy's dispersion formula:

$$n = \frac{a}{\lambda^2} + b \tag{1}$$

Where a and b are Cauchy's constant. The variation of refractive index with wavelength (of pristine and irradiated thin films) is shown in Fig 4. It is observed from Fig 4 that the calculated value of refractive index decreases as wavelength increases. It indicates normal dispersion behaviour of the composition. The refractive index gets maximized at fluence $3x10^{12}$ ions/cm^2.

The dispersion in the refractive index is described by Wemple DiDomenico relation [23, 24]

$$n_0(h\nu) = 1 + \frac{E_d E_0}{E_0^2 - (h\nu)^2} \tag{2}$$

This relation is valid when photon energy is lesser than optical bandgap. Least square fitting of $1/(n^2\text{-}1)$ on the y-axis and $(h\nu)^2$ on x-axis determines the value of dispersive energy (E_d), single oscillator energy (E_0) and static refractive index (n_0). Least square curve fitting of refractive index with energy square is shown in Fig 5. The values of $1/(n^2\text{-}1)$ for fluence $3x10^{10}$ ions/cm^2 and $1x10^{11}$ ions/cm^2 are so close. Similarly for fluence $3x10^{11}$ ions/cm^2 and $1x10^{12}$ ions/cm^2 the value of $1/(n^2\text{-}1)$ are so close. There is very little difference in the values of static refractive index (n_o) for these pairs of fluence. This fact is indicated in the inset of Fig 5. When value of static refractive index (n_o) is taken in two digits after decimal it becomes same for these pairs of fluence.

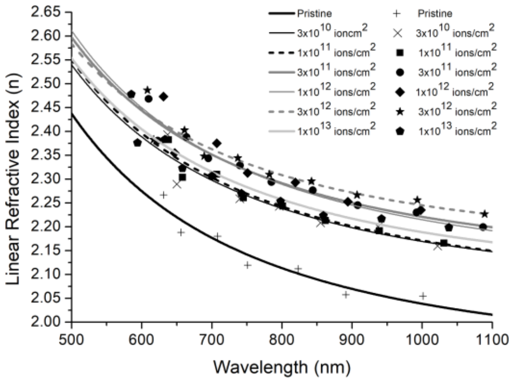

Fig. 4 Variation of refractive index with wavelength

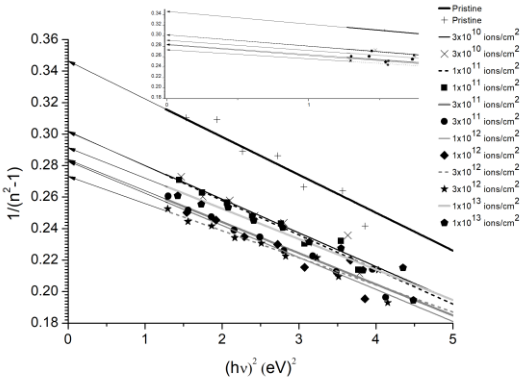

Fig. 5 Least square fitting of $1/(n^2-1)$ with $(h\nu)^2$

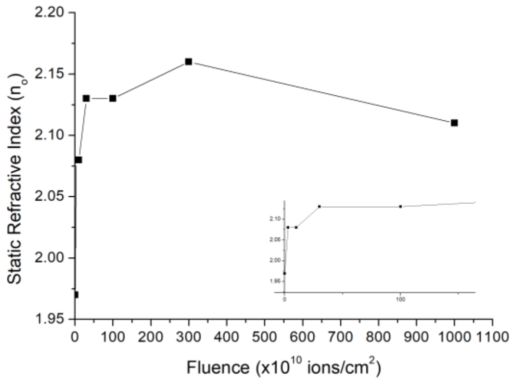

Fig.6 Variation in static refractive index with fluence

Variation in the static refractive index (n_0) with ion fluence is shown in Fig 6. The inset of Fig 6 indicates that the remain same static refractive index (n_0) for fluence $3x10^{10}$ ions/cm^2 and $1x10^{11}$ ions/cm^2. The values of n_0, E_d and E_0 are shown in Table 1, which matches well with the literature. It is clear that n_0 increases from 1.97 to 2.16 for fluence $3x10^{12}$ ion/cm^2 and then decreases to 2.11 at fluence $1x10^{13}$ ions/cm^2.

The dispersive energy E_d is measure of interband optical transition. The dispersive energy depends upon the coordination number of the cations, which are surrounded by the nearest neighbour anions. E_0 is the single oscillator energy [25]. In the present study, the dispersive energy E_d gets maximized from 10.95 eV to 14.58 eV at fluence $3x10^{12}$ ions/cm^2. Single oscillator energy E_0 also gets maximized from 3.79 eV to 3.98 eV at fluence $3x10^{12}$ ions/cm^2.

Table 1 Linear optical constant of amorphous $Ge_{22}Se_{78}$ thin films

	$n_{o\,(h\nu\to 0)}$	$\chi^{(1)}_{(h\nu\to 0)}$	E_d (eV)	E_o (eV)	E_g (eV)	$B^{1/2}$ $(cm^{-1}\,eV)^{1/2}$	K (1050 nm)
Pristine (present study)	1.97	0.230	10.95	3.79	1.99	677.38	0.03671
Pristine (literature)	2.42 [21]		18.820 [21]	3.864 [21]	1.85 [21, 22]		
$3x10^{10}$ ions/cm^2	2.08	0.264	12.44	3.75	1.98	671.87	0.02841
$1x10^{11}$ ions/cm^2	2.08	0.264	12.29	3.71	1.97	645.20	0.02931
$3x10^{11}$ ions/cm^2	2.13	0.280	13.34	3.79	1.96	643.50	0.02847
$1x10^{12}$ ions/cm^2	2.13	0.281	13.19	3.73	1.95	639.26	0.03454
$3x10^{12}$ ions/cm^2	2.16	0.291	14.58	3.98	1.94	615.51	0.02767
$1x10^{13}$ ions/cm^2	2.11	0.273	13.32	3.88	2.01	655.61	0.02322

Limiting value of first order susceptibility $\chi^{(1)}$ is dimensionless proportionality constant which indicates degree of polarisation in the dielectric material. It is determined from n_0 using following relation [26]:

$$\chi^{(1)} = \frac{(n_0^2-1)}{4\pi} \tag{3}$$

The first order susceptibility increases from .229 to .292 at fluence $3x10^{12}$ ions/cm^2 as shown in Table 1.

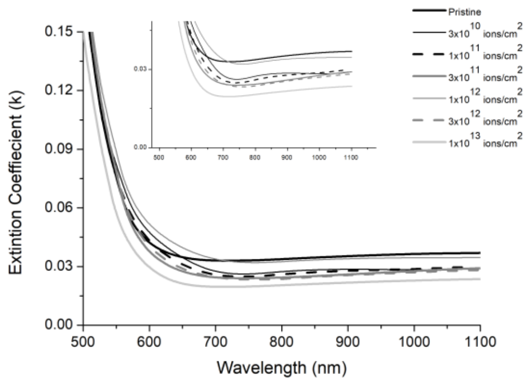

Fig. 7 Plot of extinction coefficient of pristine and irradiated thin films

The extinction coefficient is measure of attenuation of light in the intervening medium. The attenuation of light is defined using the relation $k=\alpha\lambda/4\pi$. α be the absorption coefficient of the intervening medium. Extinction coefficient of the intervening medium is determined by the relation given below

$$\alpha = \frac{1}{d} In\left(\frac{1}{x}\right) \tag{4}$$

Where d is the thickness of the thin film and x is absorbance [19, 27].

The change in extinction coefficient (k) with wavelength (λ) is shown that in Fig 7. It is clear from the figure the extinction coefficient (k) decrease with wavelength. The values of extinction coefficient (k) at wavelength 1050 nm for pristine and irradiated thin films are shown in Table 1. These values indicate that very small change is observed in extinction coefficient (k). It is clear from inset the extinction coefficient gets minimized at fluence $1x10^{13}$ ions/cm^2. It reduced from 0.03671 to 0.02322 at $1x10^{13}$ ions/cm^2 for telecommunication wavelength (1050 nm) which shown in Table 1.

The optical band gap (E_g) is determined by extrapolating the Tauc's plot for indirect band gap material. Tauc's relation for the indirect band gap material is [28]

$$\sqrt{\alpha h\nu} = \sqrt{B}(h\nu - E_g) \tag{5}$$

$B^{1/2}$ is the Tauc's parameter. It is a measurement of disorder ($B^{1/2}$ α 1/width of localized states, for $\alpha \geq 10^4$ cm^{-1}). The variation in $B^{1/2}$ and optical band gap upon 80 MeV Si SHI irradiation can be understood on the basis of Davis –Mott model [29] and cohesive energy which is later explained in Raman analysis. According to Davis-Mott model an increase in disorder increases width of localized states in forbidden regions which is responsible for reduction in Tauc's parameter and optical band gap. Similarly when disorder decreases width of localized states also decreases so Tauc's parameter and band gap increases. It is clear evidence from Fig 8 and Table 1 till fluence $3x10^{12}$ ions/cm^2 disorder increases hence width of localized increases so band gap reduces from 1.99 eV to 1.94 eV and Tauc's parameter reduces from 677.38 $(cm^{-1}eV)^{1/2}$ to 615.51 $(cm^{-1}eV)^{1/2}$. Further at fluence $1x10^{13}$ ions/cm^2 disorder starts decreasing hence width of localized states decreases so band gap increases to 2.01 eV and Tauc's parameter increases to 655.61 $(cm^{-1}eV)^{1/2}$.

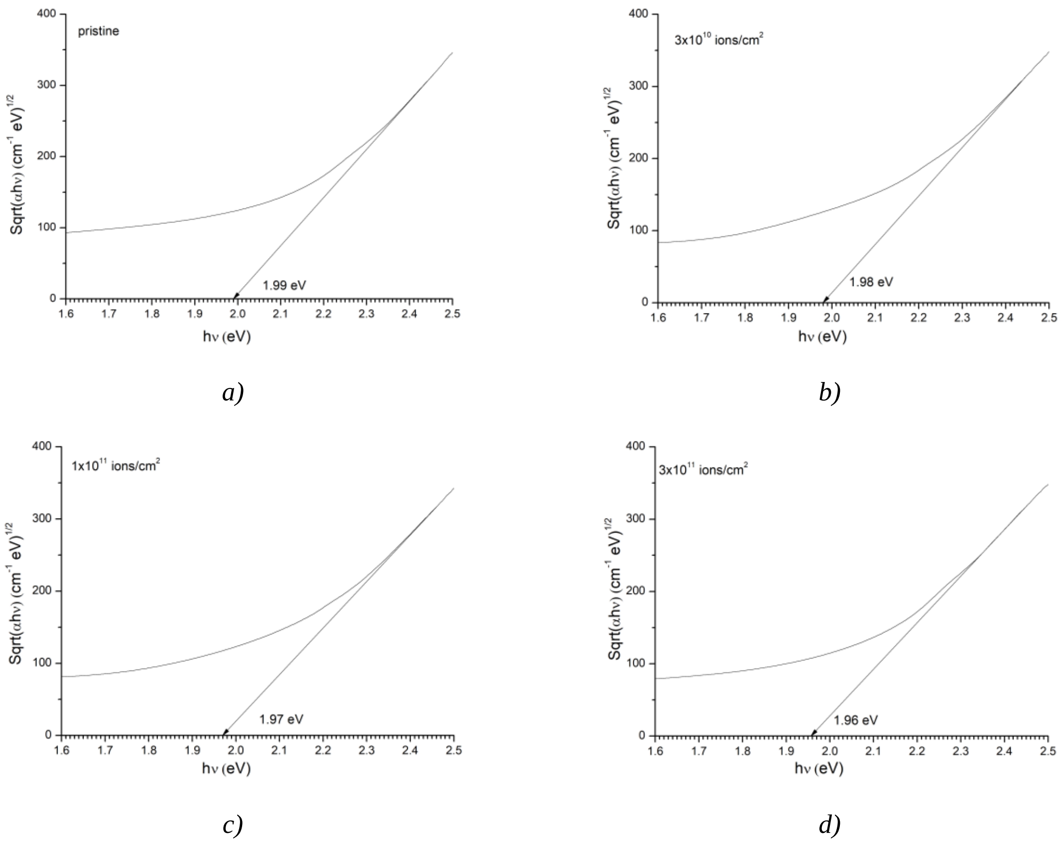

Fig. 8.1 Tauc's plot for pristine and irradiated thin films:
(a) pristine; (b) $3x10^{10}$ ions/cm^2; (c) $1x10^{11}$ ions/cm^2; (d) $3x10^{11}$ ions/cm^2

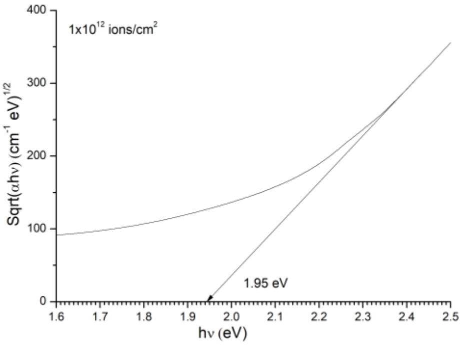

e)

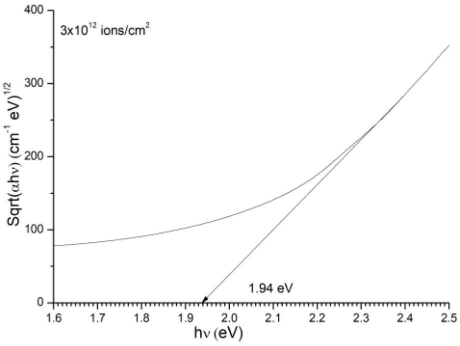

f)

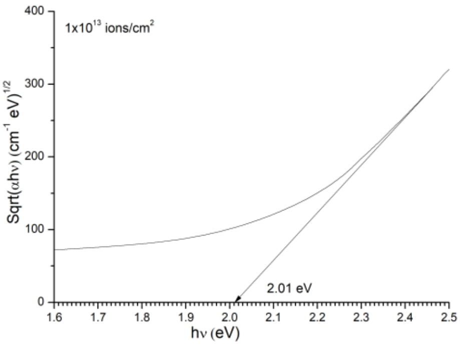

g)

Fig. 8.2 Tauc's plot for pristine and irradiated thin films:
(e) $1x10^{12}$ ions/cm^2; (f) $3x10^{12}$ ions/cm^2 8; (g) $1x10^{13}$ ions/cm^2.

3.5 Nonlinear optical analysis

The third order nonlinear susceptibility ($\chi^{(3)}$) is determined by the Miller's formula [15, 16]. The formula given by Miller was

$$\chi^{(3)} = \frac{A}{(4\pi)^4}(n_0^2 - 1)^4 \tag{6}$$

Where A=$1.7x10^{-10}$ [esu].

Table 2 exhibits that the value of the non-linear susceptibility increases from $4.737x10^{-13}$ [esu] to $12.248x10^{-13}$ [esu] up to the fluence $3x10^{12}$ ions/cm^2. Non-linear susceptibility changes due to ion irradiation because the structure of thin films is changed due to ion irradiation which is shown in Raman measurement.

Table 2 Nonlinear optical constant of pristine and irradiated a-$Ge_{22}Se_{78}$ thin films in long wavelength limit

	$\chi^{(3)}$ (10^{-13} [esu])	n_2 (10^{-11} [esu])
pristine	4.737	8.038
$3x10^{10}$ ions/cm^2	8.244	8.212
$1x10^{11}$ ions/cm^2	8.223	8.378
$3x10^{11}$ ions/cm^2	10.512	8.545
$1x10^{12}$ ions/cm^2	10.669	8.716
$3x10^{12}$ ions/cm^2	12.248	8.895
$1x10^{13}$ ions/cm^2	9.457	7.696

The change in optical band gap is responsibile for the change in the nonlinear refractive index n_2. The nonlinear refractive index determined by the relation which has given by the Ticha and Tichy [17]

$$n_2[esu] \sim \frac{\bar{A}}{E_g^4} \tag{7}$$

Where $\bar{A}$ = 1.26x10^{-9} [esu (eV)^4]

The variation in the nonlinear refractive index is shown in table 2. The nonlinear refractive index increases from 8.038x10^{-11} [esu] to 8.895x10^{-11} [esu] up to the fluence 3x10^{12} ions/cm^2. The nonlinear refractive index is changed due to the structural modification which produced by the ion irradiation. This fact can be explained from Raman analysis.

3.6 Raman analysis

Fig. 9 shows Raman plots for pristine and irradiated (3x10^{13} ions/cm^2) thin film. Raman plot of the pristine thin film exhibits four peaks at 195 cm^{-1} (peak I), 215 cm^{-1} (peak II), 236cm^{-1} (peak III), and 262 cm^{-1} (peak IV). Raman plot of 80 MeV Si SHI irradiated $Ge_{22}Se_{78}$ thin film exhibits three peaks at 196 cm^{-1} (peak I), 213 cm^{-1} (peak II), and 258 cm^{-1} (peak III). Dwivedi *et al.* reported three peaks in a-$Ge_{21.5}Se_{78.5}$ pristine thin film at 201 cm^{-1} (peak I), 215 cm^{-1} (peak II), and 263 cm^{-1} (peak III). According to the study, the peak at 201 cm^{-1} (peak I) was $Ge(Se)_{4/2}$ corner sharing tetrahedral (CS), the peak at 215 cm^{-1} (peak II) was vibration of Se atoms in the four-member rings composed of two edge-sharing tetrahedral (ES), and peak at 263 cm^{-1} (peak III) was Se-Se bonds in Se chains [10].

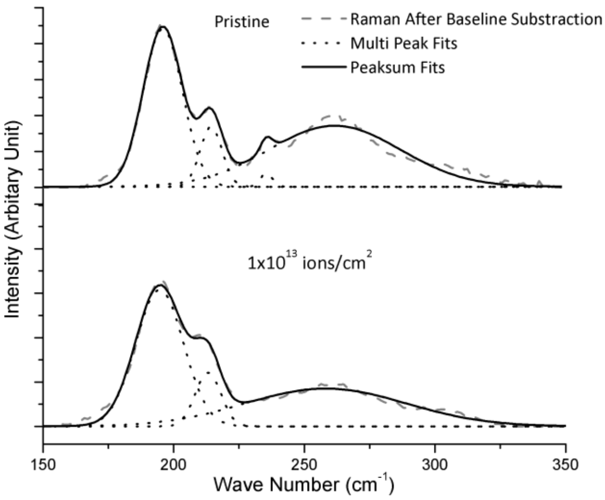

Fig. 9 Raman plots for Pristine and irradiated thin films

Jackson *et al.* reported the structure corner sharing and edge-sharing in a-$GeSe_2$ sample in their study by the first principal method [32]. Nemec *et al.* reported peaks in range 245- 250 cm^{-1} as stretching mode of Ge-Ge bond vibration (Ethane like unit) in a-GeSe thin film [33]. Tronc *et al.* and Garrido *et al* also report the similar results [34, 35]. On the basis of previous study in pristine $Ge_{22}Se_{78}$ thin film, four peaks are assigned. The peak at 195 cm^{-1} (peak I) exhibits due to $Ge(Se)_{4/2}$ corner sharing tetrahedral (CS). The peak at 215 cm^{-1} (peak II) exhibits due to vibration of Se atoms in the four-member rings composed of two edge sharing tetrahedral (ES). The peak at place 236 cm^{-1} (peak III) exhibits due to stretching mode of Ge-Ge bond vibration (Ethane like unit). The peak at 262 cm^{-1} (peak IV) exhibit due to Se-Se bonds in Se chains.

Table 3 Raman peak details for pristine and irradiated ($1x10^{13}$ ions/cm^2) thin films

Peak details	Pristine			Irradiated ($1x10^{13}$ ions/cm^2)		
	Peak position (cm^{-1})	width	Relative Area	Peak position (cm^{-1})	width	Relative Area
Peak I: $Ge(Se)_{4/2}$ corner sharing tetrahedral (CS)	195	15.15	0.395	196	18.37	0.468
Peak II: Se atoms in the four member rings composed of two edge sharing tetrahedral (ES)	215	8.49	0.084	213	9.37	0.098
Peak III: Stretching mode of Ge-Ge (Ethane like unit)	236	4.54	0.010			
Peak IV: Se-Se bonds in Se chains	262	50.85	0.511	258	61.65	0.434

It is clear from the Table 3 that due 80 MeV Si SHI irradiation on thin film the peak I at 195 cm^{-1} shifted to 196 cm^{-1}. The relative area under the curve is increased from .395 to .468 and width increased from 15.15 to 18.37.The peak at 215 cm^{-1} is shifted to 213 cm^{-1}, and relative area under the curve is increased from .084 to .098 and width increased from 8.49 to 9.37. The peak at 236 cm^{-1} is vanished. This indicates that due to 80 MeV Si SHI, the homopolar Ge-Ge bonds are completely destroyed. The position of the peak at 262 cm^{-1} is shifted to 258 cm^{-1}, but the relative area under the curve decreases from .511 to .434, and width increases from 50.85 to 61.65. It indicates that due to 80 MeV, Si SHI-irradiation some Se-Se bonds in Se chains is destroyed. Hence due to Si SHI irradiation on amorphous $Ge_{22}Se_{78}$ thin film corner sharing tetrahedral bonds and edge-sharing bonds are increased. Se-Se bonds in Se chains are decreased and Ge-Ge homopolar bonds are vanished. The bond energy of Ge-Se Bond is 49.4 kcal/mol. The bond energy of Se-Se bond is 44 kcal/mol. The bond energy of Ge-Ge bond is 37.6 kcal/mol. The cohesive energy of the pristine $Ge_{22}Se_{78}$ thin film is 45.52 kcal/mol and the irradiated thin film at fluence $1x10^{13}$ ion/cm^2 is 47.06 kcal/mol. The increase in cohesive energy is responsible for the increase in optical band gap. The polarizability of the thin film is increases due to increment in hetropolar Ge-Se corner sharing (CS) and edge sharing (ES) bonds. So the linear refractive index, linear susceptibility, nonlinear refractive index and third order nonlinear susceptibility is increased at fluence $1x10^{13}$ ions/cm^2.

4. Conclusions

Following facts are concluded, for pristine and 80 MeV Si SHI irradiated $Ge_{22}Se_{78}$ chalcogenide thin films for six different fluence ($3x10^{10}$ ions/cm^2, $1x10^{11}$ ions/cm^2, $3x10^{11}$ ions/cm^2, $1x10^{12}$ ions/cm^2, $3x10^{12}$ ions/cm^2 and $1x10^{13}$ ions/cm^2)

Amorphous nature of the $Ge_{22}Se_{78}$ thin film is retained after irradiation at highest fluence. In amorphous $Ge_{22}Se_{78}$ thin films, the upper limit of ion fluence to modify the properties of the thin film is below fluence $1x10^{13}$ ions/cm^2 because starting of destruction in the thin film as seen in SEM image at this fluence.

The static refractive index, linear susceptibility, third order susceptibility and the nonlinear refractive index is achieved maximum at fluence $3x10^{12}$ ions/cm^2. Further increase in ion fluence causes reduction in the value of these parameters.

The optical band gap and Tauc's parameter get minimized at fluence $3x10^{12}$ ions/cm^2. Further increase in ion fluence the values of these parameter increases.

Optical analysis indicates that due to the effect of 80 MeV Si SHI irradiation till fluence $3x10^{12}$ ions/cm^2 disorders in the film increases so the width of localized states increases hence

Tauc's parameter decreases and optical band gap also decreases. Further at fluence $1x10^{13}$ ions/cm^2 disorder in film starts decreasing so the width of localized states decreases hence Tauc's parameter increases and optical band gap also increases. The Raman analysis support that the cohesive energy of irradiated thin film at fluence $1x10^{13}$ ions/cm^2 increases hence band gap increases.

Raman analysis indicates that due to the effect of 80 MeV Si SHI irradiation at fluence $1x10^{13}$ ions/cm^2 the number of polarized molecules $Ge(Se)_{4/2}$ corner sharing tetrahedral (CS) and edge sharing tetrahedral (ES) increases so polarizability of thin film increases hence linear refractive index, nonlinear refractive index, linear susceptibility and third order susceptibility increases.

The fluence $3x10^{12}$ ions/cm^2 is technically important for developing optical/photonic applications because optical parameters are optimized at this fluence.

Acknowledgement

The author is thankful to IUAC, New Delhi for providing beam time and characterization facilities via BTR-4 (MS 56402). In addition, author is thankful to Dr. Ambuj Tripathi (Scientist G, IUAC, New Delhi) for coordinating in the experiment and useful discussions.

References

[1] Y. Chen, F. Wang, H. Xu, S. Ren, H. Gu, L. Wu, W. Wang, L. Feng, Chalc. Lett. **14** (1), 1 (2017).
[2] V. Vinaykumar, S. Shajii, D. Avellaneda, T. K. D. Roy, G. A. Gastillo, J. A. A. Martinez, B. Krishnan, Sol. Energy Mater. Sol. Cells **164**, 19 (2017).
[3] J. M. P. Almeda, E. C. Barbano, C. B. Arnold, L. Misuguti, C. R. Mendonca, Opt. Mat. Exp. **7**(1), 93 (2017).
[4] M. I. Sayyed, G. Lakshminarayana, M. A. Mahdi, Chalc. Lett. **14** (2), 43 (2017).
[5] R. Rodriguez, B. Poulter, M. Gonzalez, F. Ali, L. D. Lau, M. Mangern, Mater. Sci. Appl. **8**(2), 188 (2017).
[6] P. Sharma, N. Sharma, S. Sharda, S. C. Katyal, V. Sharma, Prog. Solid State Chem. **44** (4), 131 (2016).
[7] J. H. Lee, W. H. Lee, J. K. Park, J. H. Yi, S. Y. Shin, B. J. Park, B. So, J. Heo, J. H. Choi, H. J. Kim, Y. G. Choi, J. Non-Cryst. Solids **431**(41), 41 (2016).
[8] P. Boolchand, D. G. Georgive, B. Goodman, J. Optoelectron. Adv. Mat. **3**(3), 703 (2001).
[9] P. Boolchand, X. Feng, W. J. Bresser, J. Non-Cryst. Solids **293 -295**, 348 (2001).
[10] P. K. Dwivedi, S. K. Tripathi, A. Pradhan, V. N. Kulkarni, S. C. Agarwal, J. Non-Cryst. Solids **266 – 269**, 924 (2000).
[11] D. K. Awasthi, G. K. Mehta, Swift Heavy Ions for Materials Engineering and Nanostructuring, Springer, Netherlands, 2011.
[12] R. Chauhan, A. Tripathi, K. K. Srivastava, Prog. Nat. Sci.: Mater. Int. **24**, 239 (2014).
[13] M. S. Kamboj, G. Kaur, R. Thangaraj, D. K. Awasthi, J. Phys. D: Appl. Phys. **35**, 477 (2002).
[14] A. Kumar, S. K. Tripathi, P. K. Kulriya, A. Tripathi, F. Singh, D. K. Awasthi, J. Phys. D: Appl. Phys. **43,** 095302 (2010).
[15] C. J. Chen, J. C. Huang, H. S. Chou, Y. H. Lai, C W. Chang, X. H. Du, J. P. Chu, T. G. Nieh, J. Alloys Compd. **483**, 337 (2009).
[16] D. Lesueur, A. Dunlop, Rad. Eff. Def. Sol. **126**, 163 (1993).
[17] R. Maboudian, Surf. Sci. Rep. **30**(6), 207 (1998).
[18] J. F. Ziegler, SRIM-2008, http://www.srim.org., Last Retrieved on March 12, 2017.
[19] R. Swanepoel, J. Phys. E: Sci. Instrum. **16**, 1214 (1983).
[20] R. Swanepoel, J. Phys. E: Sci. Instrum. **17**, 896 (1984).
[21] A. M. Farid, Egypt. J. Sol. **25**(1), 25 (2002).
[22] S. Solieman, M. M. Hafiz, A. Hamid A., A. Sehly, A. N. A. Alfaqeer, J. Taibah Univ. Sci.

8, 282 (2014).
[23] S. H. Wemple, Phys. Rev. B **7**, 3767 (1973).
[24] S. H. Wemple, M. DiDomenico, Phys. Rev. B **3**(4), 1338 (1971).
[25] E. R. Skordeva, J. Optoelectron. Adv. Mat. **1**(1), 43 (1999).
[26] H. Ticha, L. Tichy, J. Optoelectro. Adv. Mat. **4**(2), 381 (2002).
[27] R. Chauhan, A. Tripathi, A. K. Srivastava, K. K. Srivastava, Chalc. Lett. **10** (2), 36 (2013).
[28] J. Tauc, Amorphous and Liquid Semiconductors, Plenum Press, London and New York, 1974.
[29] N. F. Mott and E. A. Davis, Clarendon, Oxford, 1979.
[30] C. Wang, Phys. Rev. B **2**(6), 2045 (1970).
[31] J. J. Wynne, Phys. Rev. B **178** (3), 1295 (1969).
[32] K. Jackson, A. Briley, S. Grossman, D. V. Porezag, M. R. Pederson, Phys. Rev. B **60** (22), R14 985 (1999).
[33] P. Nemec, J. Jedelsky, M. Frumar, M. Stabl, Z. Cernosek, M. Velcek, Philos. Mag. **84** (9), 877 (2004).
[34] P. Tronc, M. Bensoussan, A. Brenac, Phys. Rev. B **8** (12), 5947 (1973).
[35] J. M. C. Garrido, A. Piarristeguy, R. L. Parc, M. A. Urena, M. Fontana, B. Arcondo, A. Pradel, Chalc. Lett. **10**(11), 427 (2013).